Proceedings of the IASS Annual Symposium 2019 – Structural Membranes 2019
Form and Force
7 – 10 October 2019, Barcelona, Spain
C. Lázaro, K.-U. Bletzinger, E. Oñate (eds.)

Buckling strength of timber grid shell roof with steel connections considering rotational stiffness

Shun NAKAJIMA[a], Yuki TERAZAWA , Toru TAKEUCHI*
Toshiyuki OGAWA , Yoshihiro YAMAZAKI , Hiroyasu SAKATA

*Tokyo Institute of Technology
O-okayama 2-12-1-M1-29, Meguro-ku, Tokyo 152-8550, Japan
Takeuchi.t.ab@m.titech.ac.jp

[a] Former Graduate student, Tokyo Institute of Technology (NIHON SEKKEI. INC.)

Abstract

In this paper, the authors propose effective steel connections to achieve high bending stiffness and strength for timber grid-shell structures and confirm their performance through real size mock-up tests. In light of the test results, the buckling strengths of 24 m-span timber grid-shell roof structures with and without diagonal bracing roofs are discussed. The theoretical buckling strength including the rotational stiffness at connections is derived using a continuum shell analogy and compared with the results of discrete FEM analyses. Reduction factor equations of buckling strength as a function of in-plane/out-of-plane bending stiffness ratio and rotational stiffness are proposed, and their validity is confirmed.

Keywords: Grid shell, Timber-steel composite, Connection, Buckling, Continuum shell analogy

1. Introduction

In recent years, lattice shell roofs have become popular on timber structures to create a long span space that is both lightweight and aesthetically pleasing. This research proposes several types of steel connections for timber lattice shells that will improve structural performance and architectural appearance. The out-of-plane flexural strength and rotational stiffness of the proposed connections are examined by performing full-scale experiments. Based on the test results, the elastic buckling strength of 24 m-span timber grid shells with and without diagonal bracing roofs are discussed. Their theoretical buckling strength including the rotational stiffness at connections are derived using a continuum shell analogy and compared with the results of discrete FEM analyses. Finally, the reduction factor equations of buckling strength as a function of in-plane/out-of-plane bending stiffness ratio of the timber member and two directional rotational stiffness at the connection are proposed, and the validity of the equations is confirmed.

2. Mock-up test of timber-steel connections

The dimensions of the mock-up single-layer timber lattice shell are assumed to be 24 m × 24 m × 3.2 m, as shown in Figure 1. In this type of single-layered grid shell, the rotational stiffness at connections significantly affects their buckling strength. To achieve reliable connections with high bending stiffness and strength, three types of hybrid connections using steel elements are proposed, as shown in Figure 2. In Figure 2(a), rectangular laminated timber members are fixed to a tee flange section with lag screws. The tee length is set to be 1.5 times the height of the timber member (300 mm) and is referred to as TB300. TB440 has the same configuration but uses a tee length of 2.0 times the height of the timber member (Figure 2(b)). A connection using an H-

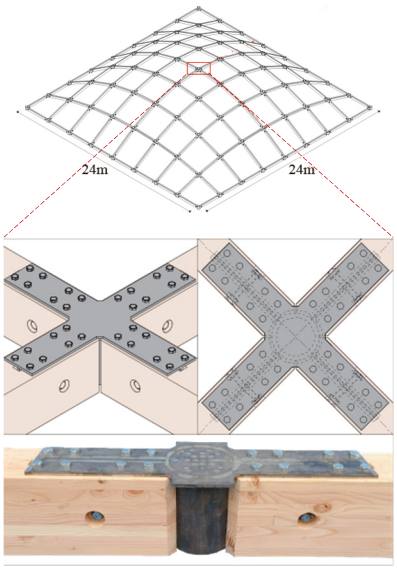

Figure 1: Latticed shell roof with timber-steel hybrid connections

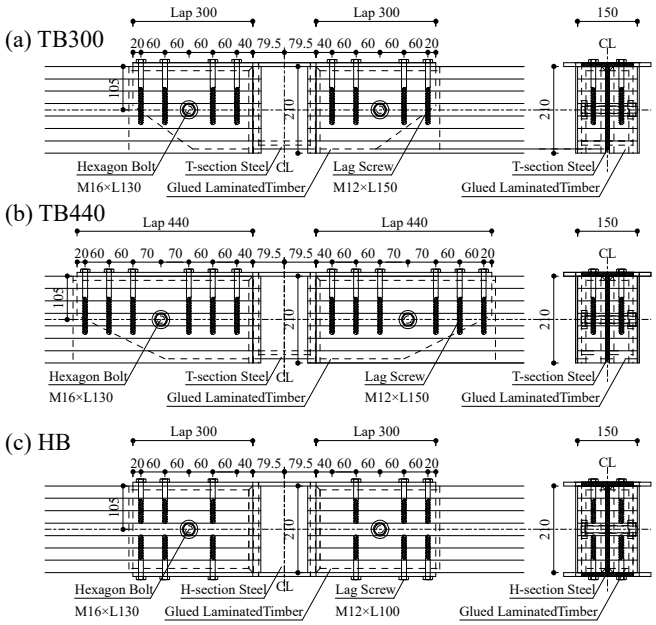

Figure 2: Hybrid connection types

bracket grasping timber member between two flanges with lag screws is referred to as HB (Figure 2(c)). These connections have resistance to out-of-plane bending moments owing to the pull-out force of the lag screws and bearing force between the timber members and the steel flanges. Tests on three specimens for each type of connection are conducted to confirm the rotational stiffness, flexural strength, and fracture mode with respect to out-of-plane and in-plane bending.

Monotonic bending tests for each connection type are conducted to confirm their bending stiffness and strength. The test setup is shown in Figure 3. The size of the timber members and connections are designed assuming the 24 m grid shell shown in Figure 1, and the material used for the specimens are shown in Table 1(a) and (b). Laminated timber members are composed of Canadian pine lamina of grade E105-F300 (E=10.5 GPa, F=30 MPa). Three specimens are tested in each connection along the out-of-plane (strong) axis in the positive and negative directions [1] and in the in-plane (weak) axis [2]. The test results are summarized in Table 2. In general the stiffness is higher in TB440, and the strength is higher in HB. The normalized rotational spring at connection $\kappa = K_\theta l/EI$ ranges between 10 and 20, and the bending strength against the timber member M_{max}/M_b is between 0.37 and 0.87, which is much higher than in conventional timber connections.

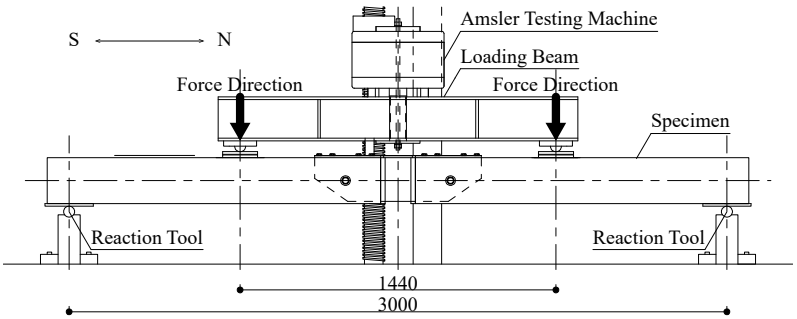

Figure 3: Setup of bending test for connections

3. Elastic buckling analyses of grid shell including connection stiffness

Using the test results, the buckling strength of a 24 m × 24 m-span grid shell roof as shown in Figure 4 is investigated as a function of the sectional stiffness ratio I_z/I_y and the connection

Table 1 Characteristic value of constituent material

(a) Glued laminated timber

Tree species	Composition	Strength grade	Direction	Bending Young's modulus (kN/mm^2)	Bending strength (N/mm^2)	Moisture content (%)	Specific gravity (-)
Douglas fir	Specific symmetric	E105-F300	Out-of-plane	16.9	64.2	9.9	0.55
			In-plane	15.2	48.9		

(b) Steel connection

Part	Steel grade	Young's modulus (kN/mm^2)	Yield strength (N/mm^2)	Tensile strength (N/mm^2)
Web	SM490A	2.09×10^2	346	511
Flange				

Table 2 Rotational stiffness and bending strength obtained by the experiment

	Out-of-plane (positive)			Out-of-plane (negative)			In-plane (negative)		
connection type	TB300	TB440	HB	TB300	TB440	HB	TB300	TB440	HB
Average of rotational stiffness K_θ (kNm/rad)	5870	11012	5377	7311	7369	5377	697	1295	1438
Coefficient of variation of 3 samples CV	0.25	0.30	0.27	0.34	0.44	0.27	0.33	0.11	0.18
Normarized rotational stiffness κ	11.6	21.8	10.7	14.4	14.6	10.7	-	-	-
Average of maximum bending strength M_{max} (kNm)	13.0	20.7	30.2	28.88	26.19	30.2	13.0	15.6	15.8
Coefficient of variation of 3 samples CV	0.04	0.12	0.04	0.06	0.10	0.04	0.12	0.03	0.06
M_{max}/M_b	0.37	0.59	0.87	0.55	0.59	0.87	0.20	0.24	0.25

stiffness ratio $K_{\theta z}/K_{\theta y}$. The following parameters are used: 1) The roof is set as either a "Grid model" without diagonals or a "Braced model" with steel rod diagonals. The load is assumed to be evenly distributed; 2) The half subtended angle φ uses values of 20º, 30º, 40º, 50º; 3) Connections are modeled as either detailed model (D) or simple model (S); 4) The cross-sectional shape is either square (S193, I_z/I_y=1.0) or rectangular (R240, I_z/I_y =0.18) with the same I_y; 5) The out-of-plane rotational stiffness of the connection is varied between rigid (R), TB300(T3), TB440

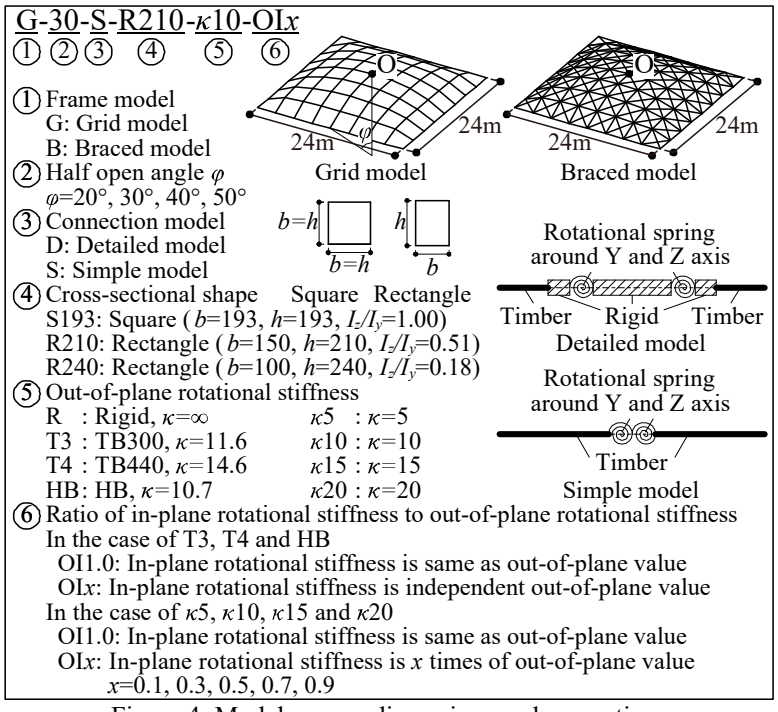

Figure 4: Model names, dimensions and properties

(T4), HB (HB), with κ=5 (κ 5), κ=10 (κ 10), κ=15 (κ 15), κ=20 (κ20); 6) Ratio of the in-plane rotational stiffness of the connection to out-of-plane rotational stiffness is varied between $K_{\theta z}/K_{\theta y}$ =1.0 (OI1.0) and $K_{\theta z}/K_{\theta y}$=0.1, 0.3, 0.5, 0.7, 0.9 (OIx, x=0.1, 0.3, 0.5, 0.7, 0.9). For T3, T4 and HB, the connection stiffness values shaded in Table 2 are used. The half subtended angle φ is defined at the ridge of the roof. No initial imperfection is assumed. The properties used for the tested connections are shaded in Table 3.

A push-over analysis including geometric nonlinearity under incremental arc-length method control is carried out, together with buckling eigenvalue analyses. Results with the simple model (S) give more conservative values than the detailed model (D). Parts of the obtained results are shown in Figure 5. When I_z/I_y is reduced (Figure 5(a)) and $K_{\theta z}/K_{\theta y}$ is reduced (Figure 5(b)), the elastic buckling strength P_{cr} is reduced. From Figure 5(b), the buckling strength of tested connections (OIx) is estimated to be reduced to approximately half of those with a rigid connection (R). Examples of the buckling modes at the point of elastic buckling are shown in Figure 6.

Table 3 Member properties of studied lattice shell

Parts	Material	Cross-sectional shape	Moment of inertia for Y axis I_y (mm^4)	Moment of inertia for Z axis I_z (mm^4)	Ratio of moment of inertia I_z/I_y (-)	Young's modulus E (kN/mm^2)	Shear modulus G (kN/mm^2)
Lattice member	Specific symmetrical composition glulam E105-F300	Square (S193) 193.1×193.1	1.16×10^8	1.16×10^8	1.00	13.1	0.87
		Rectangle (R210) 150.0×210.0		5.91×10^7	0.51		
		Rectangle (R240) 100.5×240.0		2.03×10^7	0.18		
Brace	SS400	Rod φ9	322	322	1.00	2.05×10^2	78.8

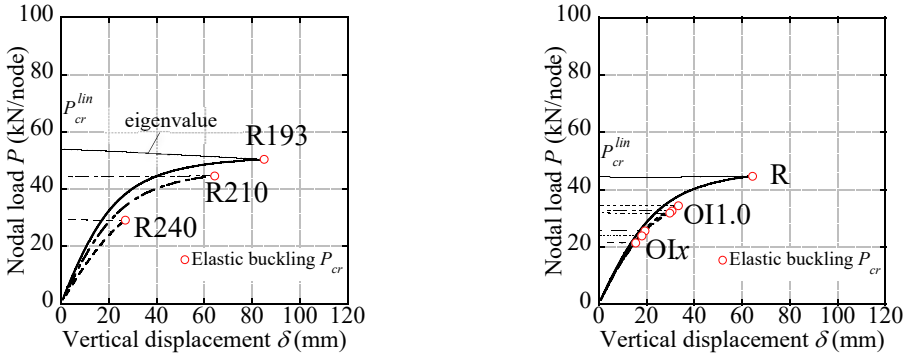

(a) Effect of sectional proportion I_x/I_z (R) (b) Effect of spring ratio $K_{\theta x}/K_{\theta z}$ (R, T3, T4, HB)

Figure 5: Elastic buckling strength with different out-of-plane/in-plane stiffness (G-30-S)

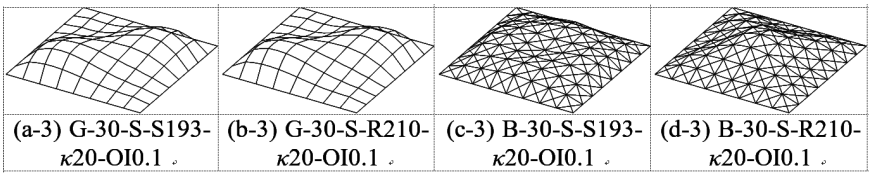

(a-3) G-30-S-S193-κ20-OI0.1 (b-3) G-30-S-R210-κ20-OI0.1 (c-3) B-30-S-S193-κ20-OI0.1 (d-3) B-30-S-R210-κ20-OI0.1

Figure 6: Elastic buckling modes (G,B-30-S-S193,R210-κ20-OI0.1)

4. Buckling strength evaluation using continuum shell analogy

Buckling strength evaluation formulae are derived using a continuum shell analogy. The stiffness of

the continuous shell plate can be expressed as follows.

In-plane: $\begin{Bmatrix} n_x \\ n_y \\ n_{xy} \end{Bmatrix} = \begin{bmatrix} K_{1111} & K_{1122} & 0 \\ K_{1122} & K_{2222} & 0 \\ 0 & 0 & K_{12} \end{bmatrix} \begin{Bmatrix} \varepsilon_x \\ \varepsilon_y \\ \gamma_{xy} \end{Bmatrix}$ (1a) Out-of-plane $\begin{Bmatrix} m_x \\ m_y \\ m_{xy} \end{Bmatrix} = \begin{bmatrix} D_{1111} & D_{1122} & 0 \\ D_{1122} & D_{2222} & 0 \\ 0 & 0 & D_{12} \end{bmatrix} \begin{Bmatrix} \kappa_x \\ \kappa_y \\ \kappa_{xy} \end{Bmatrix}$ (1b)

From the balance of complementary strain energy, each component can be expressed using the equations in Table 4. For K_{1111}=K_{2222}(=K) and D_{1111}=D_{2222}(=D), elastic buckling strength P_{cr}^{lin} of the Grid model and the Braced model can be expressed by Eq. (2) ([3], [4]).

$$P_{cr}^{lin} = \frac{4l^2}{R^2}\sqrt{\frac{2\left(D + D_{1122} + D_{12}\right)}{2/\left(K + K_{1122}\right) + 1/K_{12}}} \tag{2}$$

In the Grid model, K_{1122}= D_{1122}=0 and K_{12}/K is negligible, Eq.(2) can be reduced to Eq.(3).

$$P_{cr}^{lin} = \frac{4l^2}{R^2}\sqrt{2\left(D + D_{12}\right)K_{12}} \tag{3}$$

For G and torsional effects, D_{12}/D is negligible in timber, so Eq.(3) can be further reduced to Eq. (4).

$$P_{cr}^{lin} = \frac{4l^2}{R^2}\sqrt{2DK_{12}} \tag{4}$$

In recommendations from the AIJ [4], the following buckling strength reduction factors due to the connection stiffness are introduced. However, the effects of I_z/I_y and $K_{\theta z}/K_{\theta y}$ are not included.

$$P_{cr(\kappa)}^{ela} = \alpha_0 \times \beta(\kappa) \times P_{cr(\infty)}^{lin} \tag{5}$$

Average: $\beta(\kappa) = \begin{cases} 0.47\log_{10}(\kappa) + 0.34 & (1 \le \kappa \le 10 \quad : \text{Low stiffness}) \\ 0.19\log_{10}(\kappa) + 0.62 & (10 \le \kappa \le 100 \quad : \text{Moderate stiffness}) \\ 1.0 & (100 \le \kappa \quad : \text{High stiffnes}) \end{cases}$ (6)

Minimum: $\beta(\kappa) = \begin{cases} 0.365\log_{10}(\kappa) + 0.28 & (1 \le \kappa \le 100 : \text{Low and moderate stiffness}) \\ 1.0 & (100 \le \kappa \quad : \text{High stiffness}) \end{cases}$ (7)

where, α_0 is a knock-down factor due to imperfection and geometric nonlinearity (≅ 0.5). From Eq. (2), the following reduction factor equations considering the effects of sectional proportion I_z/I_y are proposed, where, I_z/I_y=m, and $K_{\theta z}/K_{\theta y}$=$n$.

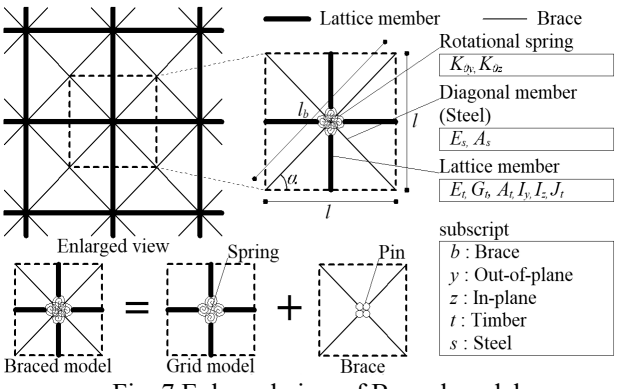

Fig. 7 Enlarged view of Braced model

Table 4 Rotational stiffness of each connections

Effective stiffness	Grid model	Braced model
$K_{1111}(=K)$	$\frac{E_t A_t}{l}$	$\frac{E_t A_t}{l} + \frac{E_s A_s}{\sqrt{2}l}$
K_{1122}	0	$\frac{E_s A_s}{\sqrt{2}l}$
$K_{2222}(=K)$	$\frac{E_t A_t}{l}$	$\frac{E_t A_t}{l} + \frac{E_s A_s}{\sqrt{2}l}$
K_{12}	$\frac{1}{l^3/(6E_t I_z) + l^2/K_{\theta z}}$	$\frac{1}{l^3/(6E_t I_z) + l^2/K_{\theta z}} + \frac{E_s A_s}{\sqrt{2}l}$
$D_{1111}(=D)$	$\frac{1}{l/E_t I_y + 2/K_{\theta y}}$	$\frac{1}{l/E_t I_y + 2/K_{\theta y}}$
D_{1122}	0	0
$D_{2222}(=D)$	$\frac{1}{l/E_t I_y + 2/K_{\theta y}}$	$\frac{1}{l/E_t I_y + 2/K_{\theta y}}$
D_{12}	$\frac{G_t J_t}{l}$	$\frac{G_t J_t}{l}$

$$\gamma_i = P_{cr(\kappa)}^{lin} \Big/ \left(P_{cr(\kappa)}^{lin} \big|_{m=1} \right) \tag{8}$$

Grid model: $$\gamma_{i.g}^{con}(\kappa) = \sqrt{\frac{1/(1+2/\kappa)+a_m}{1/(1+2/\kappa)+a_1} \cdot \frac{2/\lambda_1^{\,2}+1/6+(1/n)(1/\kappa)}{2/\lambda_m^{\,2}+1/(6m)+(1/n)(1/\kappa)}} \tag{9}$$

Braced model: $$\gamma_{i.b}^{con}(\kappa) = \sqrt{\frac{\dfrac{1}{1+2/\kappa}+a_m}{\dfrac{1}{1+2/\kappa}+a_1} \cdot \frac{\dfrac{2}{1+2s_1}\dfrac{1}{\lambda_1^{\,2}}+1\Big/\left\{1\Big/\left(\dfrac{1}{6}+\dfrac{1}{n}\dfrac{1}{\kappa}\right)+s_1\lambda_1^{\,2}\right\}}{\dfrac{2}{1+2s_m}\dfrac{1}{\lambda_m^{\,2}}+1\Big/\left\{1\Big/\left(\dfrac{1}{6m}+\dfrac{1}{n}\dfrac{1}{\kappa}\right)+s_m\lambda_m^{\,2}\right\}}} \tag{10}$$

When the connection is rigid, $\kappa = \infty$ and $1/\kappa = 0$. Eq. (10) describes the Grid model and Eq. (11) the Braced model:

$$\gamma_{i.g}^{con}(\infty) = \sqrt{\frac{1+a_m}{1+a_1} \cdot \frac{2/\lambda_1^{\,2}+1/6}{2/\lambda_m^{\,2}+1/(6m)}} \tag{11}$$

$$\gamma_{i.b}^{con}(\infty) = \sqrt{\frac{1+a_m}{1+a_1} \cdot \frac{\{1/(1+2s_1)\}\left(2/\lambda_1^{\,2}\right)+1/\left(6+s_1\lambda_1^{\,2}\right)}{\{1/(1+2s_m)\}\left(2/\lambda_m^{\,2}\right)+1/\left(6m+s_m\lambda_m^{\,2}\right)}} \tag{12}$$

$$a_m = G_t J_t \Big/ \left(E_t I_{ty}\right) = (4/5)\, jm \tag{13}$$

$$\lambda_m^{\,2} = A_t l^2 \big/ I_y = 12 l^2 m / b^2 \tag{14}$$

$$s_m = E_s A_s \Big/ \left(\sqrt{2} E_t A_t\right) = E_s A_s \Big/ \left(\sqrt{2} E_t h^2 m^{1/2}\right) \tag{15}$$

The values obtained from Eq. (9), (10) are compared with FEM analyses in Figure 8. In the grid model, Eq. (9) results in more conservative values than the numerical results. In the braced model, Eq. (10) overestimates for a lower I_z/I_y, but generally matches the numerical analyses results. This error is caused because the shear stiffness K_{12} of the roof panels in the Braced model is underestimated when neglecting axial deformations of the timber chords.

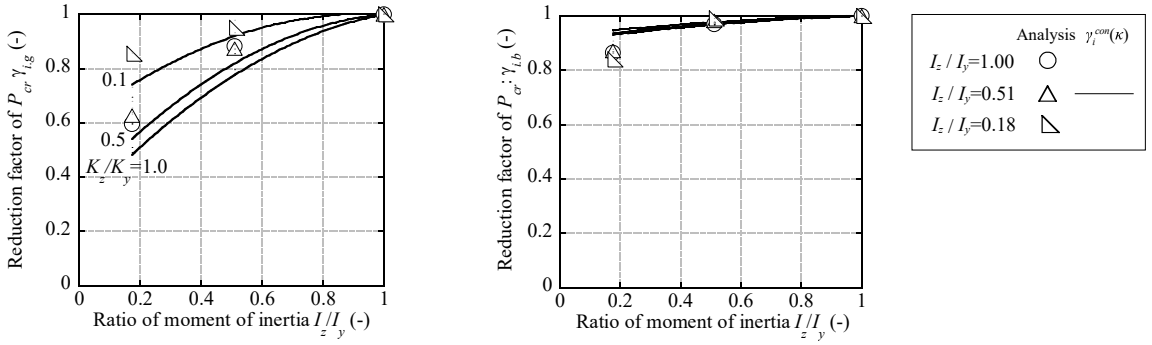

(a) Grid model (κ=10) (b) Braced model (κ=10)

Figure 8: Reduction factor of buckling load (φ=30º)

From Eq. (2), the reduction factors including the effects of $K_{\theta z}/K_{\theta y}$ can be expressed as follows.

Grid model: $$\beta_{ik.g}^{con}(\kappa) = \sqrt{\frac{1/(1+2/\kappa)+a_m}{1+a_m} \cdot \frac{2/\lambda_m^{\,2}+1/(6m)}{2/\lambda_m^{\,2}+1/(6m)+(1/n)(1/\kappa)}} \tag{16}$$

Braced model: $$\beta_{ik.b}^{con}(\kappa) = \sqrt{\frac{\dfrac{1}{1+2/\kappa}+a_m}{1+a_m} \cdot \frac{\dfrac{2}{1+2s_m}\dfrac{1}{\lambda_m^{\,2}}+\dfrac{1}{6m+s_m\lambda_m^{\,2}}}{\dfrac{2}{1+2s_m}\dfrac{1}{\lambda_m^{\,2}}+1\Big/\left\{1\Big/\left(\dfrac{1}{6m}+\dfrac{1}{n}\dfrac{1}{\kappa}\right)+s_m\lambda_m^{\,2}\right\}}} \tag{17}$$

Eq. (16) can be also expressed as Eq. (18).

$$\beta_{ik.g}^{con}(\kappa) = \kappa\sqrt{\frac{1}{(\kappa+2)(\kappa+6\,m/n)}} \times k_g \times d_g \tag{18}$$

$$k_g = \sqrt{1+\frac{\left(2/\lambda_m{}^2\right)(6m/n)(1/\kappa)}{\left(2/\lambda_m{}^2\right)+1/(6m)+(1/n)(1/\kappa)}} \quad (19), \qquad d_g = \sqrt{1+\frac{2a_m}{1+a_m}\frac{1}{\kappa}} \tag{20}$$

In the Grid model, K_{12}/K is negligible and $1/\lambda_m{}^2 = 0$, $k_g = 1$. Because D_{12}/D is negligible and $a_m = 0$ and $d_g = 1$ in timber, then Eq.(18) becomes;

$$\beta_{ik.g}^{con}(\kappa) = \kappa\sqrt{\frac{1}{(\kappa+2)(\kappa+6\,m/n)}} \tag{19}$$

The values obtained from Eq. (16), (17) are compared with FEM analyses in Figure 9. The proposed equations generally give more conservative results for the numerical analyses. Eq. (16), (17) are also compared with Eq. (6), (7) in Figure 10. In the Grid model (Figure 10 (a)), the proposed Eq. (16) gives values between those of Eq. (6) and (7) when m=n=1, and also provides the appropriate reduction values due to $K_{\theta z}/K_{\theta y}$. In the Braced model (Figure 10 (b)), the proposed Eq. (17) gives higher estimated values than the analyses, which is caused by overestimating K_{12} and neglecting axial deformation of the timber chord. In general, the reduction due to $K_{\theta z}/K_{\theta y}$ is not significant in the braced model, and with Eq. (16) with m=n=1 gives conservative values for all the cases.

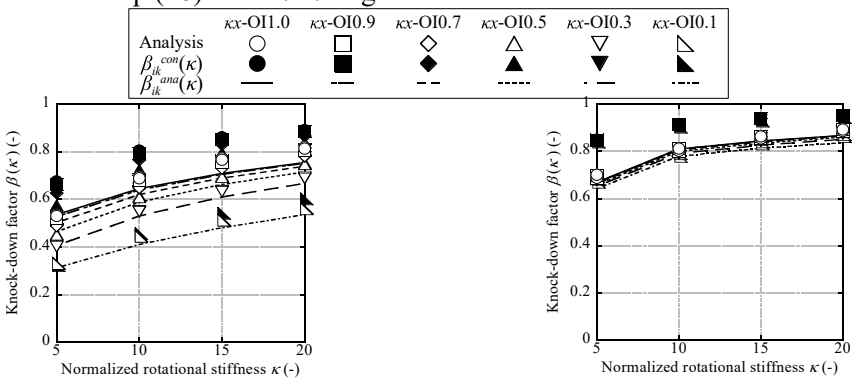

(a) Grid model (κ=10) (b) Braced model (κ=10)

Figure 9: Knock-down factor (φ=30º)

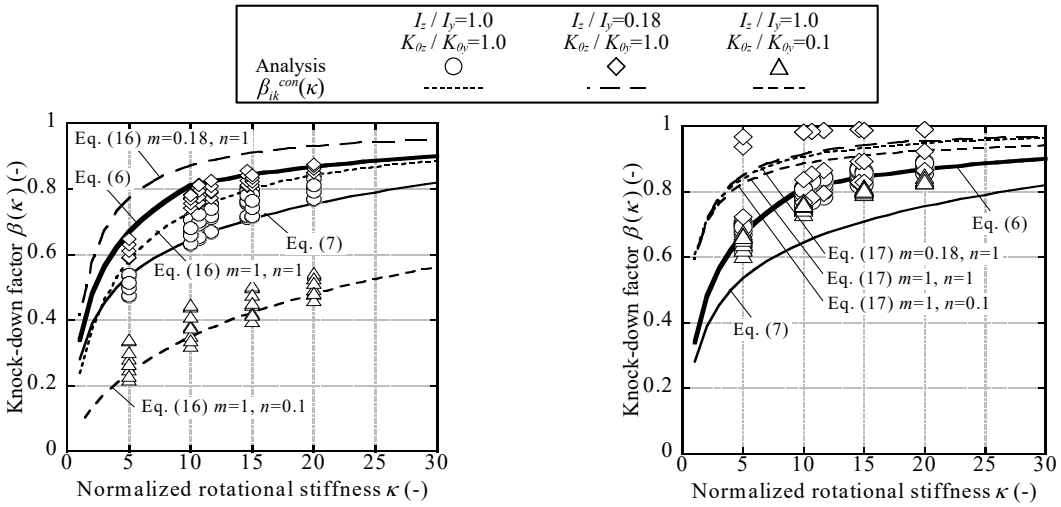

(a) Grid model (b) Braced model

Figure 10: Knock-down factor compared with AIJ recommendations

Finally, the elastic buckling strength can be expressed as Eq. (33):

$$P_{cr.ik(\kappa)}^{ela} = \alpha_0 \times \beta_{ik}^{con}(\kappa) \times \gamma_i^{con}(\infty) \times \left\{ P_{cr(\infty)}^{lin} \middle|_{m=1} \right\} \tag{33}$$

The validity of the proposed method is shown in Figure 11, compared with numerical analyses. Generally the proposed equations give consistent values with errors of approximately ±20%. For the proposed connections (κ=10–15, I_z/I_y=0.51 and $K_{\theta z}/K_{\theta y}$=0.1–0.3), β_{ik}^{con} is evaluated at approximately 0.4–0.5 for the Grid model and 0.7–0.8 for the Braced model in the case of a 24 m-span shell roof with φ=30º.

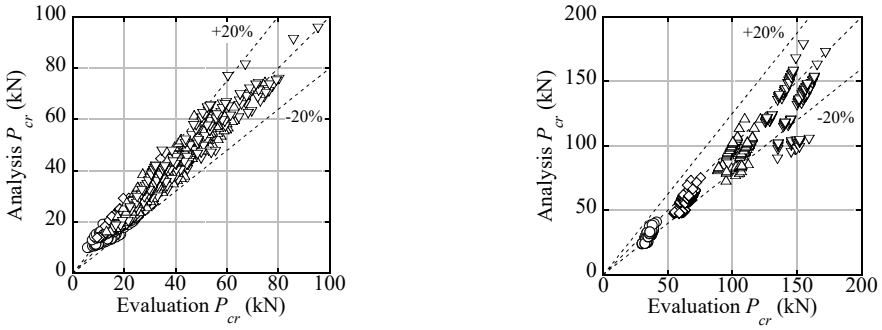

(a) Grid model (κ=10) (b) Braced model (κ=10)

Figure 11: Validity of proposed method against numerical analyses

5. Conclusions

The obtained conclusions are summarized as follows.

(1) The proposed three steel connections for timber members gives an adequate stiffness with κ=10–20 and M_{max}/M=0.37–0.87.
(2) The elastic buckling strength is reduced, especially in the Grid model, owing to the in-plane member stiffness ratio I_z/I_y and the in-plane connection stiffness ratio $K_{\theta z}/K_{\theta y}$.
(3) The buckling strength derived from the continuum shell analogy, including the effects of I_z/I_y, and $K_{\theta z}/K_{\theta y}$, gives values generally agreeing well with FEM analyses in grid-shell roofs.

Acknowledgements

The authors would like to express sincere thanks to Mr. Hiroaki Harada of NIKKEN SEKKEI Ltd., and Kenichi Hayashi of Nippon Steel Engineering Co. Ltd.

References

[1] Harada, H., Nakajima, S., Yamazaki, Y., Matsui R., Hayashi, K., Sakata, H. and Takeuchi, T.: Rotational Stiffness and Bending Strength of Steel Connections in Timber Lattice Shell, *Journal of Structural and Construction Engineering (Transactions of AIJ)*, Vol. 83, No. 746, pp. 577-587, 2018. 4 (in Japanese)

[2] Nakajima, S., Yamazaki, Y., Sakata, H., Takeuchi, T., Harada, H., and Hayashi, K.: Rotational Stiffness along Negative Out-of-plane and In-plane Directions for Steel Connections in Timber Grid-Shell Roof, *Journal of Structural and Construction Engineering (Transactions of AIJ)*, Vol. 84, No. 760, pp. 831-841, 2019. 6 (in Japanese)

[3] Kato, S., Yamashita, T.: Evaluation of elasto-plastic buckling strength of two-way grid shells using continuum analogy, *J. Space Structures*, Vol. 17, No. 4, pp. 249-261, 2002

[4] Architectural Institute of Japan: AIJ Recommendation for Design of Latticed Shell Roof Structures, 2016. 11 (in Japanese)